Biophysical Journal Volume 72 May 1997 2042–2055

Electrostatics of Lipid Bilayer Bending

Tom Chou, Marko V. Jarić, and Eric D. Siggia
Laboratory of Atomic and Solid State Physics, Clark Hall, Cornell University, Ithaca, New York 14853 USA

ABSTRACT The electrostatic contribution to spontaneous membrane curvature is calculated within Poisson-Boltzmann theory under a variety of assumptions and emphasizing parameters in the physiological range. Asymmetrical surface charges can be fixed with respect to bilayer midplane area or with respect to the lipid-water area, but induce curvatures of opposite signs. Unequal screening layers on the two sides of a vesicle (e.g., multivalent cationic proteins on one side and monovalent salt on the other) also induce bending. For reasonable parameters, tubules formed by electrostatically induced bending can have radii in the 50–100-nm range, often seen in many intracellular organelles. Thus membrane associated proteins may induce curvature and subsequent budding, without themselves being intrinsically curved. Furthermore, we derive the previously unexplored effects of respecting the strict conservation of charge within the interior of a vesicle. The electrostatic component of the bending modulus is small under most of our conditions and is left as an experimental parameter. The large parameter space of conditions is surveyed in an array of graphs.

INTRODUCTION

The membranes bounding intracellular organelles are dynamic structures, the morphology of which the cell can regulate. This happens most dramatically during mitosis, when the nuclear membrane disintegrates, probably forming vesicles (Alberts et al., 1994). Proteins destined for secretion or targeted to the plasma membrane pass from the endoplasmic reticulum (ER) to the Golgi body and thence to their target; at each step vesicles or tubular processes with diameters in the 50–100-nm range are involved in the sorting and transport (Rothman, 1994; Schekman and Orci, 1996). Similar remarks apply to endocytosis and endosomal sorting and maturation (Gruenberg and Maxfield, 1995; Trowbridge et al., 1993). The ER cisterna itself has a large tubular component (Terasaki et al., 1986), and there are tubular connections within the Golgi body (Rambourg and Clermont, 1990). Various treatments can enhance the tubulation of the membranes of Golgi and other organelles (Lippincott-Schwartz et al., 1990; Cluett et al., 1993).

Numerous plausible mechanisms have been proposed for vesicle budding or tubule formation, but often there is insufficient physical detail for a quantitative assessment of their validity. For instance, are the building blocks of the clathrin cages intrinsically curved, or do kinetic processes during budding favor five-membered over six-membered rings and thus effect closure (Shraiman, 1996)? The phase separation of wedge-shaped lipids or membrane resident proteins is also argued to play a role in vesiculation (Schekman and Orci, 1996), as is line tension between the two phases (Lipowsky, 1993). Chemical modifications to the lipids on one side of a bilayer, such as phosphorylation of inositol lipids (de Camilli et al., 1996), or cleavage of the acyl chains by phospholipases, are known to occur biologically and will promote membrane curvature. Less drastic modifications such as changes in solution pH or ionic strengths can have similar effects, because many lipids are zwitterionic and their effective charge varies with solution conditions. Furthermore, because parameters such as pH, ionic strength, temperature, and phospholipid pK_a are not independent, it is impossible to separate and quantify all of these effects.

It has long been recognized that when surface charges on the two sides are unequal, electrostatics will induce membrane curvature (Winterhalter and Helfrich, 1988, and references therein). In this article we quantify a number of less obvious influences of electrostatics on membrane bending. Symmetrically charged membranes (i.e., same surface charge on the two leaflets) will bend in response to asymmetrical screening. Thus membrane-associated proteins such as the adaptins, which mediate between the clathrin and the bilayer, could cause bending, even if the proteins are globular while free in solution. Various plausible choices for the neutral surface, with respect to which the surface charge is conserved during membrane bending, can alter even the sign of the preferred curvature resulting from a given charge or screening asymmetry. Uncharged membrane lipid components can define the neutral surface and hence modulate the electrostatic response. Finally, if the interior of a vesicle is truly electrically isolated from the exterior, a small internal charge scaling with the area can define the spontaneous curvature. The simple description of electrostatics we employ, the Poisson-Boltzmann equation, has been shown to give quantitatively accurate results for the arguably more complex problem of the binding energy

Received for publication 13 September 1996 and in final form 27 January 1997.

Address reprint requests to Dr. Eric Siggia, Laboratory of Atomic and Solid-State Physics, Clark Hall, Cornell University, Ithaca, NY 14853-2501. Tel.: 607-255-4669; Fax: 607-255-6428; E-mail: siggia@msc.cornell.edu.

Dr. Chou's present address is DAMTP, University of Cambridge, Cambridge CB3 9EW, England. E-mail: tc208@damtp.cam.ac.uk.

Dr. Jarić's permanent address is Center for Theoretical Physics, Texas A & M University, College Station, TX 77843-4242.

0006-3495/97/05/2042/14 $2.00

between a charged protein and a bilayer (Ben-Tal et al., 1996).

Even at the level of Poisson-Boltzmann theory, the electrostatic contributions to spontaneous curvature, particularly with asymmetrical (different on the two sides) and multivalent electrolytes, have not been fully quantified in the literature and are potentially significant for the concentrated electrolytes encountered in the cell. Our interest was kindled by the ubiquity of tubules within the diameter range noted above, and the possibility of getting such sizes by simple electrostatics. More attention has been paid in the physical literature to the electrostatic contribution to the curvature energy (we will generally take the total bending modulus as an experimentally determined parameter) rather than the spontaneous curvature. Low ionic strength (which enhances the electrostatic contribution to the bending modulus) was emphasized when the spontaneous curvature was computed, and symmetrical, typically monovalent electrolytes were assumed (Mitchell and Ninham, 1989; Winterhalter and Helfrich, 1988, 1992; Duplantier et al., 1990).

Our calculations are limited to the equilibrium radius of a sphere or tube with ends neglected and lipid exchange between leaflets allowed. We ignore the more subtle problem of determining the overall shape of a homogeneous vesicle with given volume, area, and leaflet area difference (related to the spontaneous curvature via Legendre transformation) (Miao et al., 1994; Seifert and Lipowsky, 1995; Mui et al., 1995). Biological systems are very inhomogeneous; they contain channels that span the membrane and enzymes that circumvent kinetic barriers to lipid repartitioning that are a feature of in vitro systems. In short, the electrostatic effects we are considering may be the physical adjunct to some of the biochemically defined actors (wedge-shaped lipids, adaptins, coatamers, etc.) involved in vesicle and tubule formation.

It should not be forgotten that electrostatic effects can be large in a biological context (Honig and Nicholls, 1995); for a surface charge of $-0.2|e|/\text{nm}^2$ (corresponding to 10% of lipids, each of size ~ 50 Å^2 possessing an electronic charge), a screening length of 1 nm, and an aqueous dielectric constant $\epsilon_w \simeq 80$, the surface potential (relative to infinity) $e\varphi \approx k_B T$, the thermal energy. Several parameters that occur repeatedly in this paper are diagrammed in Fig. 1 for a single tubule of radius R on an isolated vesicle.

In the following section we recapitulate the nonlinear electrostatic free energy (there is no unanimity among prior papers) and collect several formulae for the linearized free energy, and the leading $1/R$ term in the nonlinear free energy. We emphasize the effects of multivalent electrolytes and interleaflet coupling. The surface charge is assumed to respond to the curvature in one of two possible limits: either not at all (i.e., fixed charge per midplane area) or maximally, with charge fixed per area of each water-lipid interface (and separate reservoirs assumed for each leaflet). Equilibrium radii are very different in the two cases.

We also take literally the isolation between the interior and exterior electrolytes effected by the membrane of a giant lipid vesicle in vitro to motivate a calculation within a fixed number ensemble for the interior. Theories that assume a thermodynamic reservoir (e.g., Poisson-Boltzmann) are incorrect unless the total internal charge is set to a particular value to within $O(\epsilon_\ell/\epsilon_w)$ times the total surface charge. Deviations from this value can qualitatively change the conclusions. In the Results, we compute various quantities using realistic parameters and contrast the results and various assumptions. The concluding section reviews pertinent experiments with a view toward extracting values of parameters and supporting the various assumptions we have made.

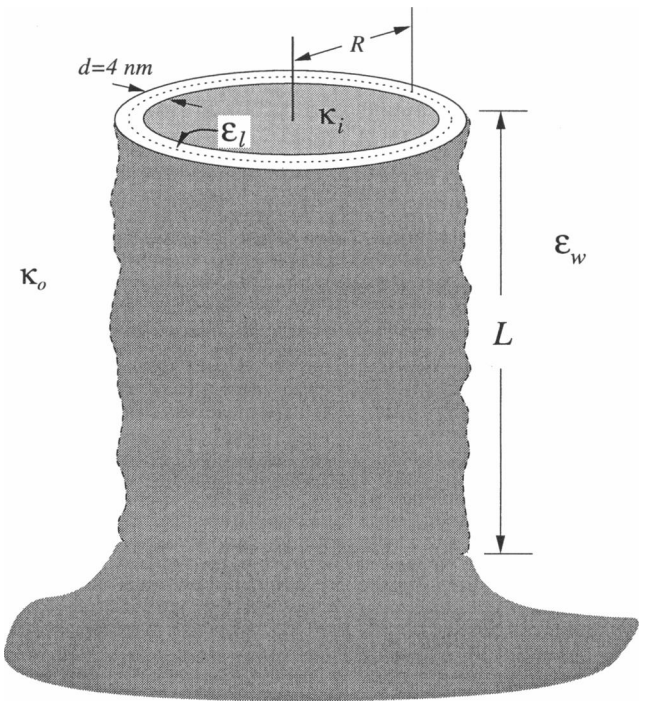

FIGURE 1 Schematic of a tubular section of a vesicle. The structure is assumed to be cylindrical, with radius R and thickness d. The interior and exterior screening lengths are κ_{i-1} and κ_{o-1}, respectively, and the dielectric constants in their respective regions are denoted by ϵ. Our calculations assume that $L \gg R$.

ELECTROSTATICS

In this study we assume that all structures are smooth on atomic-length scales and adopt the continuum limit. The problem is that of a cylindrical or spherical shell of thickness $b - a = d = 4$ nm and dielectric constant $\epsilon_\ell = 2$, embedded in an ionic solution with dielectric constant $\epsilon_w = 80$. We assume that changing the aqueous buffer ionic strength does not affect ϵ_w. These parameters approximate a lipid bilayer membrane under in vitro and in vivo conditions.

The total charge density $\rho(\vec{r})$ can be decomposed into contributions from mobile and fixed ions of type i,

$$\rho(\vec{r}) = \sum_i \rho_{i,\text{fixed}} + \sum_i \rho_{i,\text{mobile}}, \qquad (1)$$

where the fixed charge contribution resides exclusively at the lipid-water interface and can be characterized by a surface charge σ. The surface charge results from ionization of, e.g., phosphate, amine, and carboxyl groups on hydrophilic moieties of the lipids; these effective surface charges are typically negative. We do not consider spatially varying surface charges and lateral lipid phase separation; however, for dilute charge densities and smaller screening lengths, the interactions among charged lipids are expected to be minimal (Hui, 1993), and the charged component would be approximately a uniform 2D ideal gas over the entire vesicle. Details of how σ is affected by solution conditions, local membrane curvature, etc., are deferred until after results are presented.

The mobile charge density is assumed to follow a Boltzmann ensemble:

$$\rho_{i,\text{mobile}}(\vec{r}) = \rho_i^{\infty} e^{-e\beta\varphi(\vec{r})}. \tag{2}$$

where ρ_i^{∞} is the bulk concentration of species i and $\beta^{-1} \equiv k_B T$. Substituting Eq. 1 into Poisson's equation,

$$\nabla \cdot (\epsilon(\vec{r})\nabla\varphi) = -4\pi\rho(\vec{r}), \tag{3}$$

we obtain, for the electrostatic potential in the aqueous phase for the cases we treat in detail,

$$\begin{aligned}\ell^2\nabla^2\psi = n_1 \sinh\psi + n(z_+)\frac{z_+}{2}(e^{\psi} - e^{-z_+\psi}) \\ + \frac{z_-}{2} n(z_-)(e^{z_-\psi} - e^{-\psi}),\end{aligned} \tag{4}$$

where $\psi \equiv e\beta\varphi$, and n_1, $n(z_+)$, and $n(z_-)$ are the concentrations in molar units of monovalent (1:1) z_+-valent (z_+:1) and z_--valent (1:z_-) salts (e.g., NaCl, $CaCl_2$, and Na_2SO_4, respectively). Note that $z_\pm$ are positive and the concentrations refer to the molecular species (not individual ions), so the n's must be positive but are otherwise unconstrained. We have incorporated all parameter dimensions (the concentrations are relative to 1 molar) into $\ell^2 = \epsilon_w/(8\pi\beta e^2 N) = 0.0950\ \text{nm}^2$, where N is Avogadro's number per liter and $T = 300\text{K}$.

The electrostatic portion of the free energy for the lipid plus buffer system follows most readily in the limit where Eq. 4 is linearized. Thus if a surface charge is prescribed, the free energy difference between the entire lipid/solution system and the electrolytic solution without lipid surfaces is, via standard electrostatic formulas,

$$G_{e\ell} \equiv G_{\text{system}} - G_{\text{solution}} = \frac{1}{2}\int \sigma\varphi dS. \tag{5}$$

This prescription is not adequate for the nonlinear case (Sharp and Honig, 1990).

An alternative argument is then to use the expression, the variation of which yields Eq. 4 (Dresner, 1963; Sharp and Honig, 1990). Thus, with fixed surface charge,

$$\begin{aligned}G_{e\ell} = \int dS\sigma\varphi - \frac{\epsilon_w}{4\pi}\int' d^3r\left[\frac{1}{2}|\nabla\varphi|^2 + U[\varphi]\right] \\ - \frac{\epsilon_\ell}{4\pi}\int'' d^3r\,\frac{1}{2}|\nabla\varphi|^2,\end{aligned} \tag{6}$$

where the primed integral is taken only over coordinates in the aqueous solution and the double-primed integral is taken over the bilayer region ($a < r < b$) occupied by the lipid acyl chains. This equation reduces to Eq. 5 when $U[\varphi]$ is expanded to second order in ϕ (linear Poisson-Boltzmann equation). The equivalence between Eq. 6 and the thermodynamic definition of $G_{e\ell}[\sigma]$ in terms of the internal energy and entropy (ignoring electrostriction. so that the "$P - V$" term does not change) was shown by Dresner (1963) for $\epsilon_\ell = 0$, but his argument readily generalizes to our case. The equivalence of the thermodynamic definition of $G_{e\ell}[\sigma]$ and an expression involving a parameter integral was shown by Marcus (1955). We have checked that Eq. 6 can be reduced to the frequently employed charging integral $G_{e\ell} = \int d\sigma\varphi$ (Sharp and Honig, 1990), in the one-dimensional case and for all dimensions in linearized theory. Furthermore, we have explicitly verified that the $1/R$ coefficient in an expansion of $G_{e\ell}(R)/2\pi RL$ for a cylinder agrees with that found from the charging integral when membrane leaflets are uncoupled.

The free energy with fixed surface potential is just Eq. 6 with the first term omitted, $G_{e\ell}[\varphi(S)] = G_{e\ell}[\sigma] - \int\varphi(S)\sigma\, dS$. In all cases, Eq. 6 is understood to be evaluated for a stationary solution (i.e., Eq. 4).

The "potential" $U[\varphi]$ is just

$$\begin{aligned}(\ell e\beta)^2 U[\varphi] \equiv n_1(\cosh\psi - 1) \\ + n(z_+)\frac{z_+}{2}\left(e^{\psi} + \frac{e^{-z_+\psi}}{z_+} - 1 - \frac{1}{z_+}\right) \\ + n(z_-)\frac{z_-}{2}\left(e^{-\psi} + \frac{e^{z_-\psi}}{z_+} - 1 - \frac{1}{z_-}\right),\end{aligned} \tag{7}$$

in the units of Eq. 4 and vanishes as $\sigma \to 0$ to make Eq. 6 with the surface area. The surface value of φ is also to be varied, and the net coefficient of $\delta\varphi(S)$ is the usual boundary condition,

$$\sigma + \frac{\epsilon_w}{4\pi}\partial_n\varphi_w - \frac{\epsilon_\ell}{4\pi}\partial_n\varphi_\ell = 0, \tag{8}$$

at all lipid-water interfaces. The normal derivative is taken to be positive from the lipid outwards.

Linear Poisson-Boltzmann solutions

For potentials $e\beta\varphi \ll 1$, the Poisson-Boltzmann equation (Eq. 4) can be linearized. The equation to be solved with the

proper fixed charge boundary conditions is

$$\nabla^2\varphi - \kappa_{i,o}^2\varphi = 0, \tag{9}$$

where $\kappa_{i,o}$ are the effective inverse screening lengths inside or outside the vesicle ($z_\pm > 0$; cf. Eq. 4),

$$\ell^2\kappa^2 = n_1 + \frac{1}{2}n(z_+)z_+(z_+ + 1) + \frac{1}{2}n(z_-)z_-(z_- + 1). \tag{10}$$

Inside the bilayer ($a < r < b$), there are no charges ($U = 0$), and Laplace's equation holds. The cylindrically symmetrical solutions in all regions are also explicitly displayed in Appendix A. The corresponding linearized form of the free energy (Eq. 6) is $G_{e\ell} = \frac{1}{2}\int\sigma\varphi dS$, and the free energy per midplane area, $2\pi LR$, is

$$g_{e\ell} = \frac{1}{2}\sigma_a\varphi(a)\left(1 - \frac{d}{2R}\right) + \frac{1}{2}\sigma_b\varphi(b)\left(1 + \frac{d}{2R}\right). \tag{11}$$

Expressions in the decoupled limit $\epsilon_\ell/(\epsilon_w\kappa d) = 0$ have previously been found (Winterhalter and Helfrich, 1988). We will analyze consequences of the expansion

$$g_{e\ell} = C_0 + \frac{C_1}{R} + \frac{C_2}{R^2} + O\left(\frac{1}{R^3}\right) \tag{12}$$

for screening lengths appropriate to physiological conditions.

Further expanding the coefficients C_i in powers of $\epsilon_\ell/(\epsilon_w\kappa d)$, we obtain

$$C_0 = \frac{2\pi d}{\epsilon_w}\left[\left(\frac{\sigma_a^2}{\kappa_i d} + \frac{\sigma_b^2}{\kappa_o d}\right) + \frac{\epsilon_\ell}{\epsilon_w}\frac{(\kappa_i d\sigma_b - \kappa_o d\sigma_a)^2}{(\kappa_i d\kappa_o d)^2}\right] + O\left(\frac{\epsilon_\ell}{\epsilon_w\kappa d}\right)^2 \tag{13}$$

$$C_1 = \frac{\pi d^2}{\epsilon_w}\left[\frac{\sigma_b^2}{(\kappa_o d)^2}(\kappa_o d - 1) - \frac{\sigma_a^2}{(\kappa_i d)^2}(\kappa_i d - 1) + \frac{\epsilon_\ell}{\epsilon_w\kappa_i^3\kappa_o^3 d^3}\right.$$
$$(\sigma_a^2(\kappa_i^2\kappa_o - \kappa_i\kappa_o^2 - 2\kappa_o^3) + \sigma_a\sigma_b\kappa_i\kappa_o(\kappa_o - \kappa_i) + 2\sigma_b^2\kappa_o^3)$$
$$\left. + O\left(\frac{\epsilon_\ell}{\epsilon_w\kappa d}\right)^2\right], \tag{14}$$

and

$$C_2 = \frac{3\pi d^3}{4\epsilon_w}\left[\frac{\sigma_a^2}{(\kappa_i d)^3} + \frac{\sigma_b^2}{(\kappa_o d)^3} + O\left(\frac{\epsilon_\ell}{\epsilon_w\kappa d}\right)\right]. \tag{15}$$

With this notation, the total membrane bending stiffness is $2C_2 + k_m$, where k_m represents bending stiffness from nonelectrostatic (such as mechanical) contributions. When $C_1 < 0$, the membrane spontaneously curves in the sense we have assumed (b = out, a = in), and it is interesting to understanding the physical origin of the effect. For $\kappa d \ll 1$, either $\sigma_b > \sigma_a$ ($\kappa_i \simeq \kappa_o$) or $\kappa_o^{-1} > \kappa_i^{-1}$ ($\sigma_b \simeq \sigma_a$) favors bending. This prediction follows by replacing each screening layer by cylindrical capacitors; the larger charge or thicker layer will prefer the exterior, i.e., the screening charge cloud expands. In the opposite limit ($\kappa d \gg 1$), we can think of the two thin screening layers as flat; here the energy is minimized by making the layer with the greatest energy per area interior (i.e., we make it occupy the side with less area).

The influence of ϵ_ℓ is felt through the dimensionless combination $\epsilon_\ell/(\epsilon_w\kappa d)$, as expected from Eq. 8. This is always small under our conditions. Note that it is incorrect to estimate the energy as a triple of independent capacitors of thickness κ_i^{-1}, d, and κ_o^{-1}, i.e., $\sigma d/\epsilon_\ell + O(\sigma^2/\kappa\epsilon_w)$, which would make the lipid contribution appear dominant. Note also that for $\epsilon_\ell/\epsilon_w\kappa d \to 0$, C_1 is antisymmetrical with the interchange $\sigma_a \leftrightarrow \sigma_b$, $\kappa_i \leftrightarrow \kappa_o$. When coupling through the bilayer is not negligible, the antisymmetry exists only for $\kappa_i = \kappa_o$ or $\sigma_a = \sigma_b$.

Finally, we consider a scenario in which the surface charges are fixed with respect not to their physical interface area, but to an area defined by a radius in the interior of the lipid. This radius defines a "neutral surface" (Petrov and Bivas, 1984). We consider here the extreme case of conserved charge per midplane area, $A = 2\pi RL$. The physical reasons for this choice as opposed to fixed charge per area of membrane per solution interface is deferred until the Discussion. The only change to Eqs. 13, 14, and 15 is a redefinition of $\sigma_{a,b}$. In the decoupled limit, upon replacing $\sigma_{a,b} \to \sigma_{a,b}/(1 \mp d/2R)$, the coefficients C_i for $g_{e\ell}(R)$ become

$$C_1 \simeq \frac{\pi d^2}{\epsilon_w}\left[\frac{\sigma_a^2}{(\kappa_i d)^2}(1 + \kappa_i d) - \frac{\sigma_b^2}{(\kappa_o d)^2}(1 + \kappa_o d)\right], \tag{16}$$

and

$$C_2 \simeq \frac{\pi d^3}{4\epsilon_w}\left[\left(\frac{3}{(\kappa_i d)^3} + \frac{4}{(\kappa_i d)^2} + \frac{2}{\kappa_i d}\right)\sigma_a^2 + \left(\frac{3}{(\kappa_o d)^3} + \frac{4}{(\kappa_o d)^2} + \frac{2}{\kappa_o d}\right)\sigma_b^2\right], \tag{17}$$

with C_0 remaining unchanged. Note in Eqs. 16 and 17 $\sigma_{a,b}$ are now the fixed charges per midplane area. Although C_2 changes only slightly in magnitude, the behavior of C_1 is qualitatively different from Eq. 14.

Nonlinear Poisson-Boltzmann equation: solution and expansion

When the small potential condition $e\beta\varphi \ll 1$ does not hold, the full nonlinear Poisson-Boltzmann equation must be considered. It is often noted (Mitchell and Ninham, 1989; Winterhalter and Helfrich, 1992) that the first few terms of an expansion of $G_{e\ell}$ in terms of d/R or $1/(\kappa R)$ can be analytically obtained for the nonlinear theory. The first order ($1/R$) is particularly simple to derive, because one is expanding a stationary functional about its minimum and

several terms cancel. The equation to be solved is

$$-\nabla^2\varphi + \frac{\partial U}{\partial \varphi} = -\frac{\partial^2\varphi}{\partial r^2} - \frac{1}{r}\frac{\partial \varphi}{\partial r} + \frac{\partial U}{\partial \varphi} = 0, \qquad (18)$$

with the boundary conditions given by Eq. 8. Let φ_0 satisfy Eq. 18 without the $r^{-1}\partial_r\varphi(r)$ term. Upon using the boundary condition $\varphi_0 \to 0$ far from charged surfaces and $U(0) = 0$, this equation for φ_0 ($r < a$, $r > b$) can be integrated to yield

$$\frac{1}{2}(\partial_r\varphi_0)^2 - U[\varphi_0] = 0. \qquad (19)$$

For negatively charged interfaces, $\varphi_0(r = a, b)$ is negative and follows from Eq. 19 with the boundary conditions $[[\epsilon(r)\nabla\varphi_0]] = -4\pi\sigma$. Here $[[\ldots]]$ denotes the discontinuity across the charged surface. The free energy per midplane area from Eq. 6 is the sum $g_{e\ell}(R) = g_+(R) + g_-(R) + g_\ell(R)$, where g_-, g_+, and g_ℓ are contributions from the inner, outer, and lipid portions of the membrane system. One can readily show (Appendix B) that $g_\ell(R)$ contributes only even powers of $1/R$; the effect of bilayer coupling via ϵ_ℓ, however, is still felt through the surface values of φ_0 and $\partial_r\varphi_0$ determined from the boundary conditions. In Appendix B, we explicitly perform the calculation of $g_{e\ell}(R)$ to $O(1/R)$ and obtain

$$g_{el} \simeq g(\infty) + \frac{d}{2R}\left[\sigma_b\varphi_0(b) - \sigma_a\varphi_0(a) + \frac{\epsilon_w}{4\pi}\int_0^\infty (\mathcal{E}_- - \mathcal{E}_+)dz\right] + \frac{\epsilon_w}{4\pi R}\int_0^\infty (\mathcal{E}_- - \mathcal{E}_+)z\,dz \qquad (20)$$

where all inner and outer "one-dimensional" energies $\mathcal{E}_\pm \equiv \frac{1}{2}(\partial_r\varphi)^2 + U[\varphi]$ are evaluated with $\varphi = \varphi_0(z)$ and $\partial_r \to \partial_z$. The second and third terms in Eq. 20 give the $1/R$ dependence of the free energy. We have also assumed that the inner radius of the tube ($r = a$) is large enough such that $a \gg \kappa_i^{-1}$.

Nonlinear numerical calculation

For smaller R, higher order terms in $1/R$ must be taken into account, or the full nonlinear solution for $\varphi(r)$ and the corresponding free energy must be found numerically. The inner and outer solutions are matched via the surface charge-dependent discontinuous derivatives on the lipid faces, $R \pm d/2$. The two jump conditions furnish the two parameters in the solution to the Laplace equation in the bilayer, $\varphi(a < r < b) = C \ln r + D$. Integrating from $r_{max} - b \gg \kappa_o$, we introduce a parameter t such that $\varphi(r_{max}) = tK_0(\kappa_o r_{max})$ and $\varphi'(r_{max}) = -t\kappa_o K_1(\kappa_o r_{max})$ consistent with the linearized solution. The parameter t is then tuned until the solution at $r = 0$ obeys $\varphi'(0) \to 0$. Solutions for $\varphi(r)$ are then used in the nonlinear free energy (Eq. 6).

Fig. 2 plots the electrostatic potential $\varphi(r)$ calculated from both Eq. 4 and its linearized form (Eq. 9). For large radii

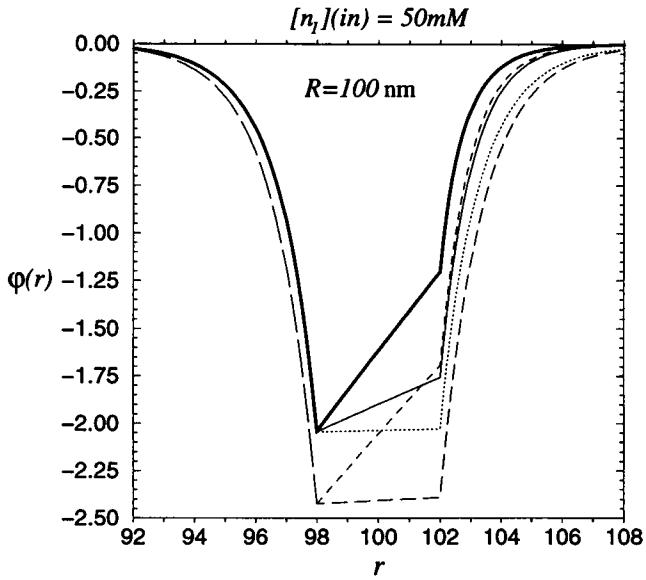

FIGURE 2 Electrostatic potential $\varphi(r)$ (k_BT/e) near negatively charged interfaces ($\sigma_a = \sigma_b = -0.2$) centered at $R = 100$ nm with 50 mM monovalent salt solution inside. The dotted and thin/thick solid curves are nonlinear Poisson-Boltzmann theory for an exterior solution of 50 mM monovalent and 33.3 mM divalent anions/cations, respectively. The long (short) dashed curves correspond to linear theory with 50 mM monovalent (33.3 mM divalent) ions comprising the exterior solution. The linearized theory in the exterior region does not distinguish between cations ($z_+ = 2$) and anions ($z_- = 2$).

($R \gg \kappa^{-1}$), both the linear and nonlinear potentials $\varphi(r)$ about the interfaces at $R \pm d/2$ are essentially those of a one-dimensional theory and are insensitive to R. However, we will show that despite the similar behavior of φ, the behaviors of $g_{e\ell}(R)$ for the linear and nonlinear cases are drastically different.

The nonlinear free energies are calculated for various values of R and fitted for large R to polynomials in R^{-1}. The $1/R$ coefficients agree with those obtained by the analytic method of the previous subsection. The $1/R^2$ coefficients are found to be drastically different from that expected from linear theory for all physiologically reasonable conditions, as previously found (see figure 1 of Winterhalter and Helfrich, 1992).

Net charge/finite volume effects

Our calculations have assumed that the solutions on both sides of the bilayer are in chemical contact with large reservoirs. For a closed vesicle with a known interior charge, the interior potential is determined by the boundary conditions at the bilayer and the zero reference potential at infinity (outside). Although it follows from elementary electrostatics, it is not widely known that the usual Poisson-Boltzmann solution, when applied to a closed vesicle, imposes a specific nonzero net internal charge; however, if the actual internal charge is different, large differences in $G_{e\ell}$ will result.

To illustrate the first assertion, use the linearized Poisson-Boltzmann solution for a flat membrane (curvature effects are unessential). Match the interior and exterior solutions through the bilayer, using the prescribed surface charges to derive the electric field within the bilayer. For a symmetrical vesicle, Gauss's law applied to a surface inside the bilayer ($a < r < b$) relates the electric field to the net interior charge (all solution charges plus σ_a) per area. Given our assumptions, this works out to

$$\sigma_{\text{interior}} = \frac{\epsilon_\ell}{\epsilon_w}\left(\frac{\sigma_a}{\kappa_i d} - \frac{\sigma_b}{\kappa_o d}\right)[1 + O(\epsilon_\ell/\epsilon_w, 1/\kappa R)] \quad (21)$$

for the vesicle. Even though on a per-volume basis this is very small, the consequences of imposing any other value inside, with the same order of magnitude, are appreciable. These concerns are not simply academic, for once a vesicle is closed the interior charge may be fixed, so even altering the exterior electrolyte (n.b. κ_o appears in Eq. 21) will lead to an imbalance between the charge present and that required under the open reservoir assumption.

For a symmetrical closed vesicle, the interior potential can be found to within an additive constant from the net charge in the solution; Gauss's law on the aqueous side of the bilayer ($r = a-$) gives the necessary boundary condition. To generalize Eq. 6 for the interior aqueous solution, we have only to use the expression given by Dresner (1963),

$$U[\varphi] = \frac{4\pi k_B T}{\epsilon_w}\sum_\alpha N_\alpha \ln V^{-1}\int_0^a e^{-q_\alpha \beta e \varphi(r)} d^3 r, \quad (22)$$

where we sum over all ions with charge eq_α, number N_α, and concentration $c_\alpha = N_\alpha/V$, where V is interior volume. By demanding stationarity under variations in φ, we find the generalization of Eq. 4,

$$\nabla^2\varphi(r) = \frac{-4\pi e}{\epsilon_w}\left[\frac{c_+ e^{e\beta\varphi(r)}}{\langle e^{e\beta\varphi}\rangle} - \frac{c_- e^{-e\beta\varphi(r)}}{\langle e^{-e\beta\varphi}\rangle}\right], \quad (23)$$

where we have specialized to monovalent ions only and $\langle \ldots \rangle$ denotes $V^{-1}\int \ldots d^3 r$. Equation 23 implies Gauss's law and is invariant under constant shifts in φ. Upon redefining the potential $\varphi(r) = \delta\varphi + \langle\varphi\rangle$, so that $\langle\delta\varphi\rangle = 0$, and expanding for $e\beta\varphi \ll 1$, we obtain

$$\nabla^2\delta\varphi(r) = \kappa_i^2\left(\delta\varphi - \frac{k_B T}{e}\frac{c_+ - c_-}{c_+ + c_-}\right). \quad (24)$$

where the definition of $\kappa_i^2 = (4\pi e^2\beta/\epsilon_w)(c_+ + c_-)$ was used to rearrange the equation. The solution to $\delta\varphi(r)$ is similar to the potentials derived from Eq. 9, except for multiplicative factors and constant shifts,

$$\delta\varphi(r < a) = -\frac{2\pi a}{\epsilon_w \kappa_i}\frac{(c_+ - c_-)e}{I_1(\kappa_i a)} I_0(\kappa_i r) + \frac{k_B T}{e}\frac{c_+ - c_-}{c_+ + c_-}, \quad (25)$$

where $I_{0,1}$ are the conventionally defined Bessel functions. It may be verified from Eq. 25 that $\langle\delta\varphi\rangle = 0$.

To illustrate most simply the order of magnitude energies involved when the interior charge is not adjusted according to Eq. 21, consider the case $c_+ = c_-$, i.e., the electrolyte plus counterions from the interior surface are together electrically neutral. The net interior charge per area as defined by a Gaussian surface interior to the bilayer as in Eq. 21 is then σ_a. Either directly from Gauss's law or from Eq. 25, the interior potential is constant and $\delta\varphi = 0$, a feature that persists in a nonlinear treatment. The interior electric field is zero, and the field in the bilayer can be found directly from the boundary condition on the inner surface, $E_\ell = 4\pi\sigma_a/\epsilon_\ell$. The interior potential is large because $E_\ell \propto 1/\epsilon_\ell$, and the outer potential to which it is matched is $\sim 4\pi\sigma_b/(\epsilon_w\kappa_o)$ and substantially smaller than $E_\ell d$. Hence, $\langle\varphi\rangle \simeq 4\pi d\sigma_a/\epsilon_\ell(1 + O(\epsilon_\ell/\epsilon_w\kappa d)$, and is a factor of ~ 40 larger than $\varphi(S)$ calculated in the previous sections, because of the ϵ_ℓ in the denominator. However, in the linear limit with $c_+ = c_-$, the free energy given by Eq. 11 still holds. The coefficients in a $1/R$ expansion are

$$C_1 = -\frac{2\pi d^2}{\epsilon_\ell}\left[\sigma_a^2 + \frac{\epsilon_\ell}{\epsilon_w\kappa_o d}\cdot\left(\frac{(\sigma_a + \sigma_b)^2}{2\kappa_o d} + \frac{3}{2}\sigma_a^2 + \sigma_a\sigma_b - \frac{\sigma_b^2}{2}\right)\right] \quad (26)$$

and

$$C_2 = \frac{2\pi d^3}{3\epsilon_\ell}\left[\sigma_a^2 + \frac{\epsilon_\ell}{\epsilon_w(\kappa_o d)^2}\cdot\left(\frac{9(\sigma_a + \sigma_b)^2}{8\kappa_o d} + 3\sigma_a^2(1 + \kappa_o d) + 3\sigma_a\sigma_b\right)\right]. \quad (27)$$

Both C_1 and C_2 are a factor of $\sim\epsilon_w/\epsilon_\ell$ larger than in the conventional theory. This is no surprise, because the interior charge is larger than Eq. 21 by a similar factor. For small ϵ_ℓ, the dominant term arises from $\sigma_a\varphi(a)$, and its sign merely says that energetically, a charged shell prefers to elongate. When the net interior charge is on the order of Eq. 21, C_1, C_2 should scale as $1/\epsilon_w$.

RESULTS

In this section we investigate the effects of charge asymmetry, ionic strength, and multivalency of the inner and outer solutions on the linear and nonlinear electrostatic energies. A free energy of the form in Eq. 6 holds for each side of the impermeable membrane. Energies and charge densities will be expressed in units of $k_B T/\text{nm}^2$ and $|e|/\text{nm}^2$, respectively. The numerical values we have chosen are representative of either physiological conditions or those used in vitro experiments with artificial vesicles; however, there are no commonly accepted standard conditions.

The form of $g_{e\ell}(R)$ is displayed in Fig. 3. Here we have considered, for simplicity, only the charge per physical leaflet area ensemble with $\sigma_a = -0.25$, $\sigma_b = -0.15$, and monovalent ions both interior and exterior to the bilayer. In

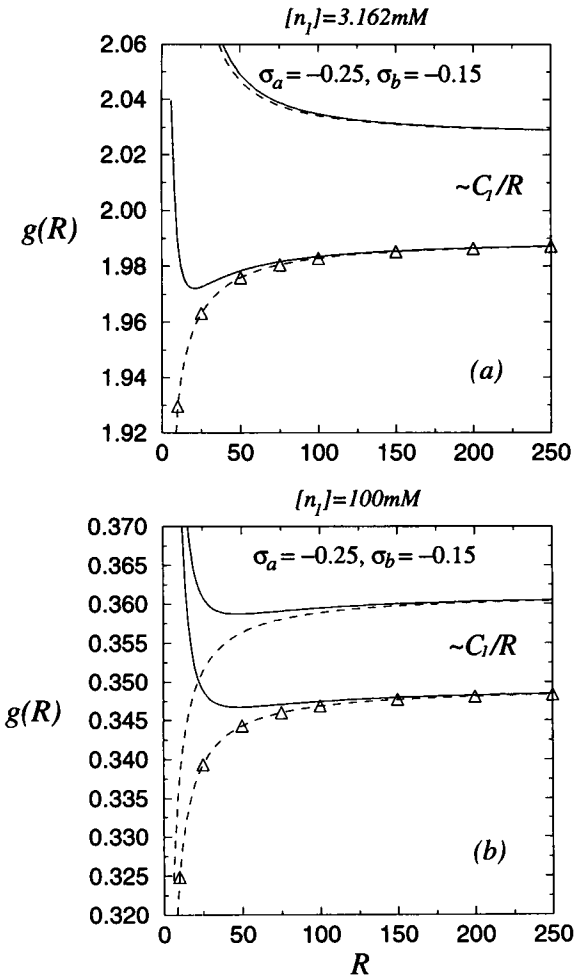

FIGURE 3 Linear and nonlinear free energies per area as a function of midplane radius for surface charges $\sigma_b = -0.15$, and $\sigma_a = -0.25$. Dashed lines represent electrostatic contributions only, solid lines depict $g_{TOT}(R) = g_{e\ell} + 6k_BT/R^2$. Linear solutions are shown in the upper pairs of curves, and nonlinear Poisson-Boltzmann solutions are shown in the lower pairs of curves (nonlinear $g_{e\ell}(R)$ are fits to the *open triangles*). (*a*) $10^{-2.5}$ M $\simeq$ 3.16 mM monovalent salt inside and outside the vesicle. For plotting purposes, the nonlinear energies have been shifted upward by $+0.8k_BT/nm^2$. (*b*) n_1 = 100 mM on both sides. The nonlinear energies have been shifted by $+0.01k_BT/nm^2$.

Fig. 3 *a* ($n_1 = 10^{-2.5} \simeq 3.16$ mM), the linear free energy $g_{e\ell}(R) = \frac{1}{2}\int\sigma(S)\varphi(S)dS$ (*dashed line*) is monotonically decreasing with increasing R, whereas the nonlinear $g_{e\ell}(R)$ has $C_1 < 0$. When ion concentration is increased as in Fig. 3 *b* (n_1 = 100 mM), nonlinear and linear results become similar in that $C_1 < 0$. In fact, for the parameters used, the nonlinear $g_{e\ell}(R)$ shows no minimum in R, implying that in the absence of other forces, the lipid tubule will collapse until the "hard wall" limit $R \simeq d$ is approached and the inner surface charge becomes a line.

However, in addition to ionic forces, other shorter-ranged electrostatic and entropic interactions lead to mechanical bending rigidities k_m. The solid lines in both graphs plot $g_{e\ell}(R) + \frac{1}{2}k_m/R^2$, with $k_m = 12k_BT$. Under realistic physical conditions, the electrostatic contributions to the $1/R^2$ terms in the free energy, $C_2 > 0$, are small compared to measured mechanical k_m values, which in uncharged vesicles fall in the range $k_m \approx 2 - 30k_BT$ (Song and Waugh, 1990; Andelman, 1995). Therefore, the total free energy for large R behaves as

$$g_{TOT}(R) \simeq C_0 + \frac{C_1}{R} + \frac{(C_2 + k_m/2)}{R^2} + O(1/R^3), \quad (28)$$

We will henceforth consider the $1/R^2$ coefficient, $C_2 + k_m/2 \simeq k_m/2$, as an independently measured stiffness, of mostly nonionic contributions, and use an intermediate approximation, $k_m \simeq 12k_BT$, where required. Any nonionic contribution to C_1 is ignored in the following, but could be added back in. The balancing of the $1/R$ and $1/R^2$ contributions controls the size scales in bilayer bending and membrane structures, such that the free energy minimizing radius is

$$R^* \simeq \frac{k_m + 2C_2}{|C_1|}, \quad (29)$$

for $C_1 < 0$, and the gain in free energy (relative to the flat state) at this radius is

$$g_{TOT}(\infty) - g_{TOT}(R^*) \simeq \frac{C_1^2}{2(k_m + 2C_2)}. \quad (30)$$

In Fig. 4, *a*, *b*, and *c*, we plot the dependence of C_1 on n_1 for three different groups of surface charges: ($\sigma_a = -0.021$, $\sigma_b = -0.019$), ($\sigma_a = -0.21$, $\sigma_b = -0.19$), and ($\sigma_a = -0.25$, $\sigma_b = -0.15$), and both surface charge ensembles. In each figure, linear theory is represented by curves that increase sharply for low n_1. The behavior of C_1 calculated from nonlinear theory is drastically different for low ion concentrations, but approaches the linear theory at high concentrations. The pair of curves ($C_1 > 0$ at large n_1) corresponding to conserved charge per midplane area remain positive. This is most easily seen in linear theory from Eq. 16 and represents the dominant effect of increasing total interior surface charge. In the charge per midplane ensemble, the inner charge σ_a increases against a deeper potential $\varphi(a)$ than σ_b decreases; this electrostatic work maintains $C_1 > 0$, thus biasing a negative radius of curvature (invaginations). Nonlinearities, as expected, mitigate these effects. Also shown is C_1 in the decoupled limit ($\epsilon_\ell/(\epsilon_w\kappa d) \to 0$), with dashed curves. We have checked that for all physically reasonable parameters, $g_{e\ell}(R)$ varies by at most only a few percent when coupling between the two interfaces (at $R - d/2$ and $R + d/2$) is neglected.

The small effect of membrane coupling (for $\epsilon_\ell = 2$, $\epsilon_w = 80$) is clearly demonstrated in Fig. 4 down to $n_1 \simeq 0.1$ mM, especially at higher surface charges (compare Fig. 4 *a* with Fig. 4, *b* and *c*), because the difference in surface potentials, $\varphi(b) - \varphi(a)$, remains relatively small as the surface potential increases in magnitude nonlinearly. Because the coupling-induced contribution of the bilayer enters through $\varphi(b) - \varphi(a)$, its relative importance diminishes as $|\sigma|$ in-

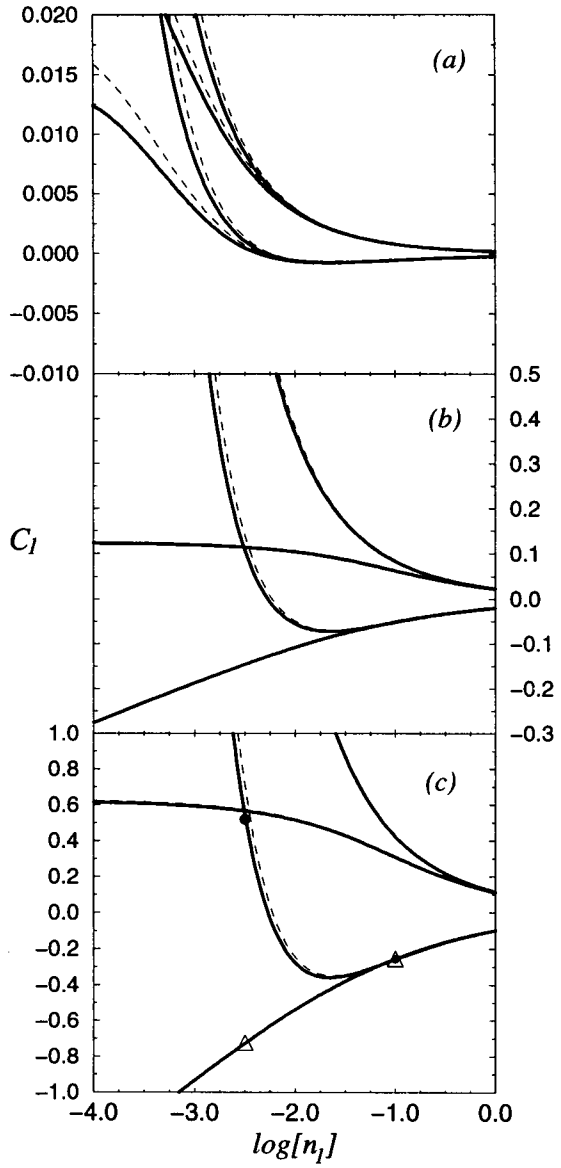

FIGURE 4 C_1 (k_BT/nm) as a function of monovalent ion concentration ($\log_{10}$ scale, equal both sides). (*a*) $\sigma_a = -0.021$, $\sigma_b = -0.019$. (*b*) $\sigma_a = -0.21$, $\sigma_b = -0.19$. (*c*) $\sigma_a = -0.25$, $\sigma_b = -0.15$. The filled circles and triangles indicate the approximations and parameters used in plotting $g_{e\ell}(R)$ in Fig. 3. Dashed (solid) curves show C_1 under decoupled (coupled) approximations. The upper set of curves in each graph ($C_1 > 0$ for large n_1) corresponds to surface charge per midplane area, whereas the lower branches ($C_1 < 0$ for large n_1) correspond to surface charge conserved with respect to area physically occupied by charges.

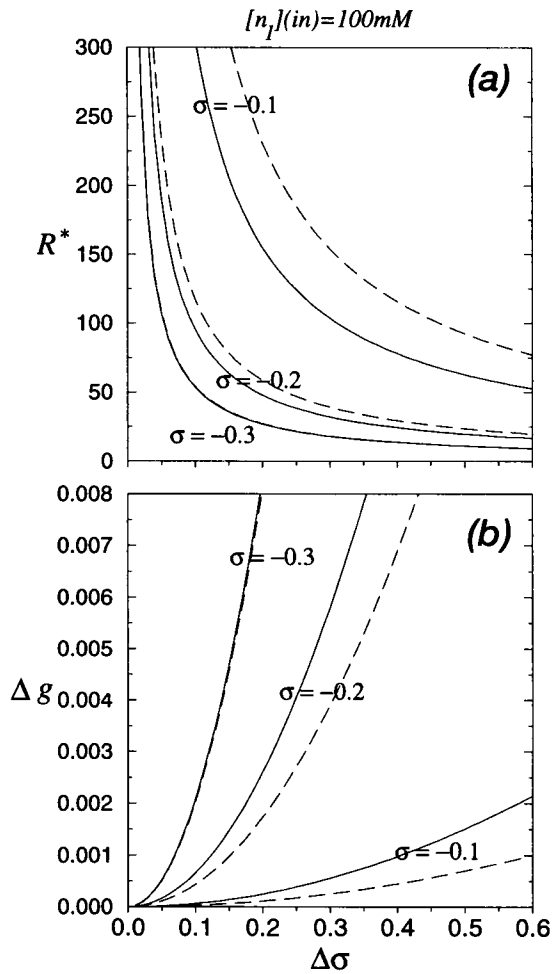

FIGURE 5 (*a*) Minimum energy radii R^* (nm) (with the assumption $k_m = i2k_BT$) plotted as a function of charge asymmetry $\Delta\sigma = (\sigma_b - \sigma_a)/(\sigma_a + \sigma_b)$ for mean charge $\sigma = (\sigma_a + \sigma_b)/2 = -0.1$, -0.2, and $-0.3|e|/nm^2$. Solid (dashed) curves represent fixed charge per leaftlet (midplane) areas. For fixed charge per midplane area, $R^* > 0$ corresponds to charge asymmetries opposite those plotted, i.e., $\Delta\sigma = (\sigma_a - \sigma_b)/(\sigma_a + \sigma_b)$. (*b*) The associated free energy changes $\Delta g(R^*)(k_BT/nm^2)$ (Eq. 30). Monovalent salt concentration is fixed at 100 mM.

creases, particularly in nonlinear theory (see Appendix B, Eq. 37). Furthermore, note that inasmuch as the interior and exterior solutions are identical, a symmetry exists, i.e., the interchange $\sigma_a \leftrightarrow \sigma_b$ leads to $C_1 \rightarrow -C_1$. The open triangles in Fig. 4 *c* indicate the parameters used in generating $g_{e\ell}(R)$ in Fig. 3.

Fig. 5 explicitly shows R^* and $g_{TOT}(\infty) - g_{TOT}(R^*)$, based on Eqs. 29 and 30 with $k_m = 12k_BT$. Thus a C_1 of order $0.1k_BT$/nm is required to electrostatically induce radii of curvatures in the ~50-nm range. For example, in the nonlinear cases plotted in Fig. 4, *b* and *c*, at a 50 mM monovalent salt concentration and conserved charge per leaflet area, Eq. 29 yields minimum free energy tube radii of 182 nm and 37 nm, respectively. The depths of these energy minima are given by Eq. 30 as 0.2×10^{-4} k_BT/nm^2 and 4.4×10^{-3} k_BT/nm^2, respectively. Similar values are obtained when charge per midplane area and the opposite charge asymmetries are considered. Coincidentally, the magnitudes of C_1 are nearly equal for the two conserved charge ensembles when $\sigma = (\sigma_a + \sigma_b)/2 = -0.3$; their magnitudes differ again as $\sigma > -0.3$. Fig. 5 shows that protuberances with radii relevant to biological systems can occur under appropriate conditions attainable experimentally in vitro and in vivo.

The surface values, $\varphi(S)$, where $|\varphi(r)|$ is a maximum, are plotted in Fig. 6, *a* and *b*, as functions of n_1 and n_2, respectively, to assess the validity of linear theory. Linear

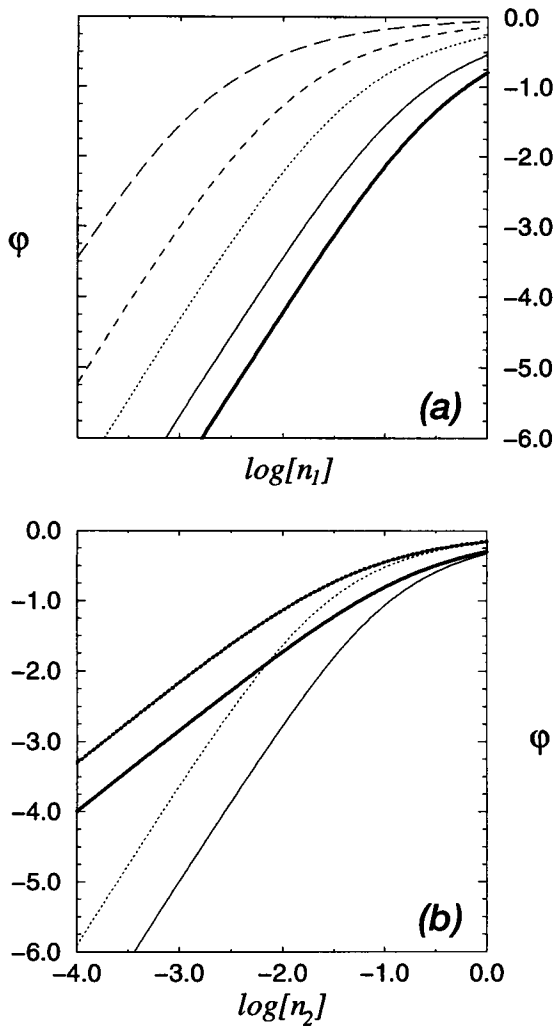

FIGURE 6 Surface electrostatic potential at a negatively charged plane interface. (*a*) $\varphi(S)$ as a function of monovalent salt concentration. Long dashed, dashed, dotted, solid, and thick solid lines denote surface charges of -0.02, -0.05, -0.1, -0.2, and $-0.3|e|/\text{nm}^2$ respectively. (*b*) Surface potential in the presence of a divalent salt solution. Thick (thin) lines indicate divalent cation (anion) solutions, and dotted (solid) lines correspond to $\sigma = -0.1$ ($\sigma = -0.2$).

theory is expected to be accurate when $ze\beta\varphi(r) \lesssim 1$, although the linear C_1 calculated in the charge per leaflet area ensemble seems to be more accurate over a larger range of ionic strength than that calculated in the charge per midplane area ensemble (see Fig. 4). The effects of divalency on $\varphi(S)$ are revealed in Fig. 6 *b*. Effects of divalent anions are quantitatively similar to those of monovalent salts, especially if we compare at the same concentration of monovalent cations, which do most of the screening. However, for divalent cations, $|\varphi(S)|$ is substantially reduced and linear theory is valid over a wider range of concentrations. The $z_+ = 2$ species is more effective at screening, because they will balance more negative surface charge $e\beta\varphi(S)$ for the same penalty in entropy of mixing incurred.

Differences in the inner and outer buffer solutions can also affect membrane bending. By simply changing the relative ionic strengths of the solutions, one can induce different screening and hence bilayer bending. For simplicity, we consider the extreme case of pure monovalent and pure divalent salt solutions. Bilayer bending due to solution asymmetry is demonstrated in Fig. 7, *a* and *b*, where C_1 is shown as a function of $\sigma = -\sigma_a = -\sigma_b$ for both surface charge ensembles (charge/leaflet area, *thin lines*; charge/midplane area, *thick lines*) for interior monovalent ion concentrations of 1, 10, and 100 mM from top to bottom within each triplet of curves. The necessary concentration of multivalent ions to achieve flaccid vesicles is assumed in the exterior solution, e.g., $2n_1^{(\text{out})} = (z_\pm + 1)n^{(\text{in})}(z_\pm)$. Here, for divalents, $n^{(\text{in})}(2) = 2n_1{}^{(\text{out})}/3 = 0.666$, 6.66, and 66.66 mM, respectively. Fig. 7 shows that divalent cations (*a*) are more effective at inducing larger curvatures (larger C_1) than divalent anions (*b*).

For small surface charges in the charge per leaflet area ensemble, linear theory (Eqs. 10 and 14) is expected to hold and yields positive (negative) slope for $C_1(\sigma)$ when n_1 is less (greater) than $(3/2 + \sqrt{2})(\ell/d)^2 M \simeq 17.3$ mM. How-

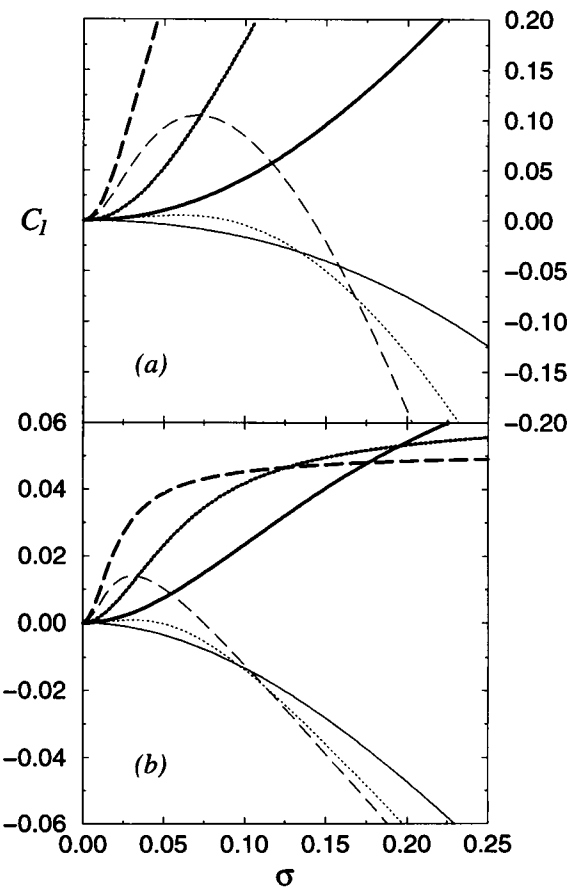

FIGURE 7 C_1 (k_BT/nm) as a function of $\sigma = -\sigma_a = -\sigma_b$ for various solution asymmetries. Monovalent salt concentration in the interior is maintained at 1, 10, and 100 mM (*dashed, dotted,* and *solid lines,* respectively), and an equiosmolar concentration (0.66, 6.66, and 66.6mM) of divalents makes up the exterior solution. Thick lines represent conserved charge per midplane area ensemble. (*a*) Exterior divalent cations, $z_+ = 2$ (e.g., $CaCl_2$). (*b*) Exterior divalent anions, $z_- = 2$ (e.g., Na_2SO_4).

ever, at larger surface charges the behavior of C_1 crosses over to a negative slope for this ensemble, especially for higher salt concentrations (see Fig. 7). Here the nonlinear screening in the membrane exterior enhances the decrease in $|\varphi(b)|$ relative to that of $|\varphi(a)|$ as σ is increased, thus increasing the electrostatic energy of the interior charge layer relative to that of the exterior, resulting in bending with $C_1 < 0$.

The values of C_1 corresponding to conserved charge per midplane area (*thick curves*) increase quadratically, with σ agreeing with linear theory, until σ becomes large enough that nonlinear effects become important and saturates C_1. The nonlinear effects are more prevalent for anions (Fig. 7 *b*), for the reasons discussed in relation to Fig. 6.

Thus we see that tuning the relative screening lengths is an effective way of inducing membrane curvature. Fig. 8 shows C_1 for surfaces of $\sigma_a = \sigma_b = -0.1$ (*thin lines*) and -0.2 (*thick lines*) as the screening in the exterior solution is scanned. Here the vesicle interior is held at 50 mM monovalent salt, whereas the exterior has a varying proportion of monovalent and divalent salt, keeping the vesicle flaccid (this requires $n_1^{(out)} = 0.050 - 3n^{(out)}(2)/2$). The various divalent mixtures required to induce positive curvature ($C_1 < 0$, tube growth), or invaginations ($C_1 > 0$) and the sensitivity of C_1 to divalent concentrations are clearly shown. Because $\sigma_a = \sigma_b$, exchange of the solutions on the two sides of the membrane interchanges $C_1 \rightarrow -C_1$.

Finally, in Fig. 9 we plot C_1 as a function of $\sigma = -\sigma_a = -\sigma_b$ for vesicles with interior monovalent salt and exterior

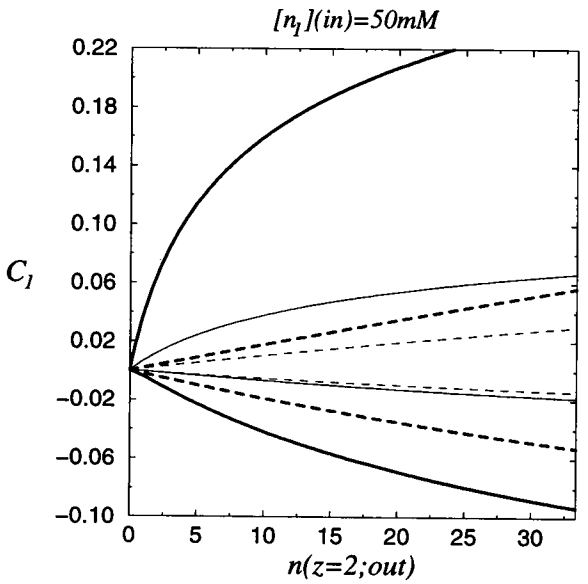

FIGURE 8 C_1 (k_BT/nm) as a function of $n(z_\pm = 2)$ in the exterior, showing how substitution of divalent for monovalent salt induces curvature. The interior solution is fixed at 50 mM monovalent salt, and the solutions are equiosmolar. Thin (thick) lines correspond to $\sigma_a = \sigma_b = \sigma = -0.1$ (-0.2). The four lower curves ($C_1 < 0$) correspond to fixed charge per leaflet area with solid (dashed) lines corresponding to divalent cations (anions). The four upper curves correspond to fixed charge per midplane area with other conventions unchanged.

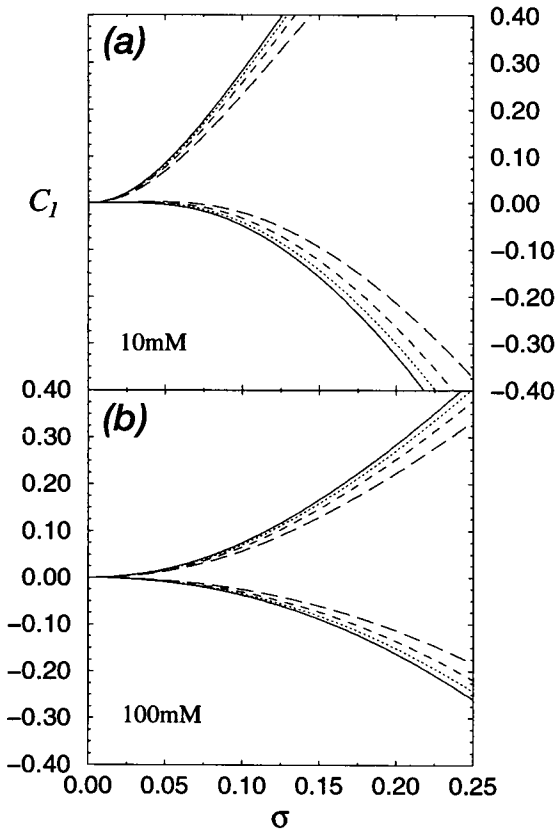

FIGURE 9 C_1 (k_BT/nm) as a function of $\sigma = -\sigma_a = -\sigma_b$ for exterior cationic multivalencies, $z_+ = 3$ (*long dashed*), 4 (*dashed*), 5 (*dotted*), and 6 (*solid lines*). (*a*) n_1(out) = 10 mM. (*b*) n_1(out) = 100 mM.

higher multivalent ions ($z_\pm > 2$). The influence of higher valencies on C_1 is modest, except at high surface charges or low total ionic strengths.

DISCUSSION AND CONCLUSIONS

In this paper we have presented calculations which suggest that electrostatic forces can control lipid membrane bending under realistic experimental and physiological conditions. Membrane deformations can be induced by an aqueous solution asymmetry between the vesicle interior and exterior, as well as by charge asymmetry between the two bilayer leaflets. Radii of curvature of the membrane bending can be in the neighborhood of 50–100 nm, typically seen in biological processes such as vesicle budding, tubulation of ER and Golgi bodies, and endo/exocytosis.

Tubulation and growth of necks from vesicles require the membrane to nucleate such protuberances. Electrostatic changes in free energy alone can yield qualitatively reasonable conditions for the formation of tubelike structures from a flat bilayer membrane. For example, if $\Delta g_{TOT}(R^* \simeq 40$ nm) $\simeq 0.0005 k_BT/\text{nm}^2$, the total free energy decrease is roughly $0.11 k_BT$/nm length. Therefore, a flat membrane is stable against tube fluctuations of height $L \lesssim 10$ nm. This critical length will be slightly greater becuase of the addi-

tional bending energy cost at the tube base; however, from experimental electron microscopy images (Mui et al., 1995), the base can be approximated with a portion of a torus of cross-sectional radius ~10 nm. Using a bending rigidity of $k_m \simeq 12k_BT$, and the fact that this toroidal section has both positive and negative curvatures, we find that the total mechanical bending rigidity is qualitatively small and does not affect the energetics appreciably, such that once a fluctuation exceeds ~10 nm, it will continue to extend and lower $g_{e\ell}$.

Magnitudes of membrane surface charges experimentally measured indicate that our canonical estimate of $-0.2|e|/nm^2$ is a reasonable physiological value. Surface charges measured in plant vesicles using particle electrophoresis and dye fluorescence range from $-0.03|e|/nm^2$ to $-0.24|e|/nm^2$ (Sack et al., 1983; Chow and Barber, 1980). These are averaged charge densities; higher concentrations of charged lipid could be recruited to incipient buds (phase separation) if electrostatics are playing a role. The numerous detailed chemical mechanisms of lipid-solvent interactions have not been modeled. The variation of lipid pK_a's with solution ionic strengths, the nonelectrostatic binding of cations to membrane surfaces, and the hydrogen bonding among lipid headgroups can all affect the effective surface charge; this is discussed by Tocanne and Teissié (1990).

The response of surface charges to bending is also crucial in determining the electrostatic contributions to the free energy. The two extreme cases examined correspond to charge distributions that are lipid tail or head controlled; these are depicted in Fig. 10. For large headgroups in which lipid packing is governed by steric and electrostatic interactions among headgroups, the surface charge is held approximately constant as the bilayer curvature is varied. Conversely, when the tails occupy a thermodynamic area larger than the heads, the surface charge is approximately fixed with respect to the area defined by the midplane of the bilayer. Furthermore, other special phases may be important in determining charge distribution. For example, if the solvent contains glycerol or alcohols, the acyl chains of PC bilayers become interdigitated (Gennis, 1989), as shown in Fig. 10 *c*. If this coupling is tight, the surface charge on the leaflets would be determined by the midplane area.

It is interesting to note that the modes of charge conservation mentioned above can be correlated with a filling parameter defined by Israelachvilli et al. (1980),

$$f = v/a\ell, \tag{31}$$

where v is the effective volume of the lipid tail, a is the thermal area of the headgroup or the tailgroup near the head, and ℓ is the vertical thermal length of the tail. For $f \simeq 1$, the lipids are schematically represented by cylinders. For $f > 1$ and $f < 1$, the lipids behave microscopically approximately as cones and inverted cones, respectively. The $f > 1$ ("tail packed") or inverted cone $f < 1$ ("head packed") structures will probably be associated with fixed surface charge with respect to midplane area and fixed surface charge with respect to leaflet interfaces ($r = a, b$) ensembles, respectively. Depending on the chemical composition of the bilayer, an intermediate neutral surface between R and a, b is also possible (Petrov and Bivas, 1984; Gennis, 1989).

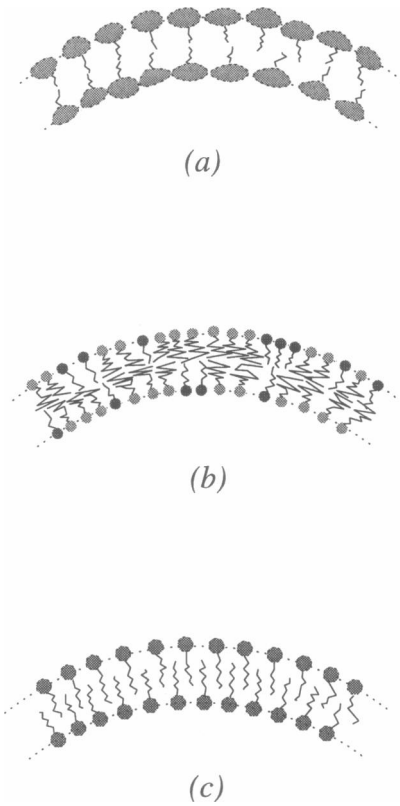

FIGURE 10 Microscopic models governing the distribution of charge and the neutral surface. (*a*) Bulky heads sterically fix charge per inner and out leaflet areas. (*b*) Small heads and entropically interacting acyl chains distribute charges at the heads according to midplane area. (*c*) Charge per midplane area preserved owing to interdigitated acyl chains.

Correlating the cartoon in Fig. 10 and the arguments above with bilayer chemistry may serve as an important guide in developing in vitro experiments and understanding biological processes. Studies of the phases of concentrated lipid solutions suggest that f is related to lipid micellular, planar, and inverted micellular structures. For example, lipids such as phosphatidylcholine, phosphatidylserine, phosphatidylinositol, phosphatidylglycerol, and sphingomyelin at nonacidic conditions and in the absence of divalent cations (Boggs, 1984) form stable planar bilayers, implying that interlipid interactions through the tailgroup and headgroup are comparable. Lysophospholipids, on the other hand, form micelles with the headgroups pointing outward into the aqueous phase, and can be modeled by inverted cones, with the cone apex at the midplane of the bilayer, commensurate with strong headgroup interactions.

In general, factors that increase the effective acyl chain area relative to that of the headgroups favors the H_{II} (inverted hexagonal) phase over the L_α (planar) phase (Gruner et al., 1985). As in the case of surface charge, chemical

conditions affect how lipids are packed in a bilayer. For example, a low pH tends to increase headgroup association through hydrogen bonding (Boggs, 1984), and cations, such as Mg^{2+} and Ca^{2+}, also decrease the size of headgroups by dehydrating them. This enhances the likelihood of the H_{II} phase. Lee et al. (1993) have qualitatively applied the lipid shape concept to the POPtdEtn/PtdEth binary lipid mixture. Under their conditions, PtdEth has a large tail area, which promotes the formation of inverted hexagonal phases in the lipid mixture (Lee et al., 1993). In our study, vesicles containing similar types of lipids may be expected to conserve surface charge with respect to midplane area $2\pi RL$.

Probably the least accurately measured parameter in bilayer electromechanical models is the coefficient of $1/R^2$ in $g_{TOT}(R)$. Measurements using various methods have yielded scattered results. For example, in phosphotidylcholines, large values of k_m are obtained when tube bending measurements are employed, intermediate values are obtained when a fluctuation mode analysis is performed, and low values are extracted when electric field deformation of spherical vesicles is analyzed (Andelman, 1995). For example, Song and Waugh (1993) measured $k_m \simeq 28k_BT$ for SOPC by mechanically pulling tethers. This value increased by about threefold when ~45% cholesterol was added. Mode fluctuation measurements by Mutz and Helfrich (1990) on lipid vesicles of ~10 μm yielded $k_m \simeq 4k_BT$, $28k_BT$, and $100k_BT$ for galactosyldiglyceride, dimyristoylphosphatidylcholine, and dimyristoylphosphatidylcholine + 30% cholesterol bilayers, respectively. Finally, electric field deformation studies by Duwe et al. (1990) on digalactosyldiacylglycerol and egg yolk PC vesicles yielded $k_m \simeq 2k_BT$ and $k_m \simeq 5k_BT$, respectively. All of these measurements were performed under neutral pH and low salt concentrations, where electrostatic contribution to the total bending rigidity ($k_m + 2C_2$) may be important. However, without careful experimental control of the solution ionic strengths (and surface charges), variation in C_2 can lead to the discrepancies reported. The enhancement of membrane bending stiffness upon surface association of uncharged polymers has also been studied by Evans (personal communication). Throughout this paper we have simply subsumed all of these effects under an intermediate value of $k_m + 2C_2 \simeq 12k_BT$, where $C_2 \ll k_m$ at the higher salt concentrations considered.

Song and Waugh (1990) also measured bending stiffnesses of artificial mixed POPS-SOPC vesicles as a function of surface charge by varying the composition of charged POPS. They found no difference in total bending stiffness for 0%, 2%, and 16% POPS ($\sim 35k_BT$). However, the solution ionic strengths and effective surface charges in these experiments were not precisely controlled, and assuming surface charges appropriate to the added amounts of POPS, even screening lengths of ~30 nm can cause C_2 to saturate at a maximum value of $\ll k_m$ (Winterhalter and Helfrich, 1992).

Experiments on artificial liposomes hitherto have not carefully considered the effects of solution ionic strength on deformation, tubulation, and budding. In the experiments of Mui et al. (1995), a pH gradient across a bilayer was used to flip lipids with different pK_a across from one leaflet to the other. Tubulation was induced, which the authors attributed to a leaflet area imbalance driven by the lipid exchange. However, as shown by Hope et al. (1989), pH-induced transport of lipids across the bilayer also changes the relative charges between the bilayer leaflets. These experiments, therefore, do not isolate the electrostatic effects we have calculated, even though, as we have shown, the electrostatic component may play a significant role in vesicle shape changes. Using natural Golgi bodies, Cluett et al. (1993) performed experiments with Brefeldin A and approximately 50 mM ion concentration. Tubules up to 7 μm in length grew when Brefeldin A was added to prevent binding of coat proteins and budding. The tubes were of the same size (~70 nm) as typical budding vesicles, suggesting that a common controlling factor, such as electrostatics, is not unreasonable.

Besides continuum electrostatics, there are numerous other chemical and biological effects that can alter the mechanical properties of a bilayer. In particular, ion binding and hydrogen bonding effects have not been considered. However, experiments hitherto have not even carefully controlled parameters that affect the electrostatics, such as solution ionic strength and surface charge. We propose that in vitro experiments on large vesicles be performed under flaccid conditions with ionic strength and that the pH be carefully measured. Systematically varying the surface charge may also be appropriate.

Our calculations have shown how adding neutral dopants to a bilayer can indirectly induce morphological changes of electrostatic origin. For example, if enough cholesterol, a rigid molecule with a relatively small headgroup, is incorporated equally in the bilayer leaflets, upon bending, phospholipid charges will be conserved with respect to a neutral surface closer to the midplane radius R, as indicated by Fig. 10, *b* and *c*. Although $k_m > 0$ is also expected to change in magnitude, the sign of C_1 is very sensitive to how charge is conserved. With asymmetry in $\sigma_{a,b}$ (Fig. 4) or interior/exterior screening (Fig. 8), the addition of cholesterol can change the sign of C_1 and determine whether tubules grow outward or invaginate. A gradient in lipid composition occurs biologically, for example, with cholesterol in the Golgi-ER membranes (Bretscher and Munro, 1993). Such membranes are constantly tubulating, budding, and recycling, and their local cholesterol content may determine the neutral surfaces that govern the electrostatic component of these processes.

We have also shown that provided a pure lipid bilayer is impermeable to ions, the conservation of charge in the interior of a closed vesicle can completely alter the electrostatic energies calculated assuming thermodynamic reservoirs. Only for a certain interior charge density specified to $O(\sigma_a/R)$ will the conventional result apply, although for a few tubes growing from a sphere of much larger area, our charge imbalance analysis should be applied to the sphere

only. For in vitro studies of pure bilayer vesicles it is experimentally difficult to control the interior charge to the required accuracy, and thus large electrostatic effects are likely to be present, at least initially, before the inner and outer solutions have equilibrated.

For total interior charge of order $\sigma_{a,b}$ times the area, the internal potential will be on the order of $(\epsilon_w/\epsilon_\ell)k_BT/e$, which is absurdly large for biological membranes, and will even will cause ions to traverse an artificial bilayer. If electrogenic ion pumps act to maintain an electronic potential difference of several k_BT across an organelle's membrane, there may still be an effect on the optimal curvature comparable to what we have calculated in the Results. Our calculations are most apt for a membrane in which pores allow small inorganic ions to equilibrate while multivalent proteins are localized to one side and control the bending.

Finally, we have verified that the effects of multivalent species ($z_\alpha > 2$) in the surrounding buffer solution are similar to those of the divalent solutions, which we have treated in more detail. This has implications for vesicle budding assisted by adaptin/clathrin or dynamin proteins, the molecular charges of which can interact and screen those at the bilayer surfaces.

APPENDIX A

The solutions to the linear equation 9 in the geometry of Fig. 1, under appropriate electrostatic boundary conditions, are displayed:

$$\varphi(r<a) = 4\pi\sigma_a\kappa_o b a K_1(\kappa_o b)\left[\frac{\epsilon}{\epsilon_w}\left(\frac{\sigma_b}{\sigma_a\kappa_o a}+\frac{1}{\kappa_o b}\right)\frac{K_0(\kappa_o b)}{K_1(\kappa_o b)} + \ln\left(\frac{b}{a}\right)\right]\frac{I_0(\kappa_i r)}{D(\kappa; a, b)}$$

$$\varphi(a<r<b) = 4\pi\sigma_b\frac{\kappa_i a b I_1(\kappa_i a)K_1(\kappa_o b)}{D(\kappa; a, b)}\ln r + \text{constant} \tag{32}$$

$$\varphi(r>b) = 4\pi\sigma_b\kappa_i a b I_1(\kappa_i a)\left[\frac{\epsilon}{\epsilon_w}\left(\frac{\sigma_a}{\sigma_b\kappa_i b}+\frac{1}{\kappa_i a}\right)\frac{I_0(\kappa_i a)}{I_1(\kappa_i a)} + \ln\left(\frac{b}{a}\right)\right]\frac{K_0(\kappa_o r)}{D(\kappa; a, b)},$$

where

$$D(\kappa; a, b) \equiv \epsilon_w\kappa_i a\kappa_o b I_1(\kappa_i a)K_1(\kappa_o b)\left[\frac{\epsilon_\ell}{\epsilon_w}\frac{1}{\kappa_o b}\frac{K_0(\kappa_o b)}{(K_1(\kappa_o b)} + \frac{\epsilon_\ell}{\epsilon_w}\frac{1}{\kappa_i a}\frac{I_0(\kappa_i a)}{I_1(\kappa_i a)} + \ln\left(\frac{b}{a}\right)\right]. \tag{33}$$

APPENDIX B

Write the solution to Eq. 18 as an expansion in $1/R$: $\varphi = \varphi_0 + \varphi_1$, where φ_0 is the solution to the one-dimensional Poisson-Boltzmann equation for a flat interface, with boundary conditions appropriate to surface charges $\sigma_{a,b}$ and $\varphi_1 = O(1/R)$. Expanding $G_{e\ell}$, for example, in the outer ($r \geq b$) and bilayer ($a < r < b$) regions, respectively,

$$\frac{G_+ + G_\ell}{2\pi L} \simeq \sigma_b b(\varphi_0(b) + \varphi_1(b)) - \frac{\epsilon_w}{4\pi}\int_b^\infty \left(\frac{1}{2}(\partial_r\varphi_0)^2 + (\partial_r\varphi_0)(\partial_r\varphi_1) + U[\varphi_0] + \varphi_1 U'[\varphi_0]\right) r\,dr \tag{34}$$

$$-\frac{\epsilon_\ell}{4\pi}\int_a^b \left(\frac{1}{2}(\partial_r\varphi_0)^2 + (\partial_r\varphi_0)(\partial_r\varphi_1)\right) r\,dr + O(1/R).$$

Using the identity $(\partial_r\varphi_0)(\partial_r\varphi_1) = \nabla\cdot(\varphi_1\nabla\varphi_0) - \varphi_1\nabla^2\varphi_0$, and recalling that to the order in R to which we are working, we can approximate $\nabla^2\varphi_0 \simeq \partial_r{}^2\varphi_0 \equiv U'[\varphi_0]$ in the first integral, one sees that the U' terms cancel. The total derivatives in both integrals reduce to surface terms that cancel $\sigma_b b\varphi_1(b)$ and the corresponding term at the inner surface when G_- is included. This is no accident, because the electrostatic boundary conditions just express the stationarity of Eq. 6 with respect to variation in the surface value of φ. In fact, because $\partial_r\varphi_0$ satisfies boundary conditions based on $\sigma_{a,b}$, $\varphi_1(a,b) \equiv 0$. Our argument does establish that φ_0 could satisfy the $R \to \infty$ boundary condition for the fixed charge per midplane area ensemble without affecting the $1/R$ coefficient. Of course, the explicit $\sigma_{a,b}$ that occurs in $G_\pm$ should be correct for the particular ensemble.

To extract the R dependence from the integrals over φ_0 we write $rdr \to \pm(R \pm d/2 \pm z)dz$ in $G_\pm$ and expand. Incidentally, this argument shows that for a sphere, the coefficient of $1/R$ is doubled, due entirely to the variation of surface area with radius. The integral within the bilayer is symmetrical about R and does not contribute to the $1/R$ coefficient. For numerical purposes it is convenient to use Eq. 19 and express the remaining integrals in Eq. 20 using φ_0, which is a monotonic function of r, as the independent variable, i.e.,

$$\int_0^\infty dz\mathscr{E}[\varphi_0] = \int_0^\infty dz(\partial_z\varphi_0)^2 = \int_{-|\varphi_0(S)|}^0 d\varphi_0\sqrt{2U[\varphi_0]}, \tag{35}$$

and similarly,

$$\int_0^\infty z\,dz\mathscr{E}[\varphi_0] = \int_{-|\varphi_0(S)|}^0 \left[\frac{1}{\sqrt{2U[\varphi_0]}}\int_{-|\varphi_0|}^0 \sqrt{2U[\varphi'_0]}d\varphi'_0\right]d\varphi_0. \tag{36}$$

The relevant boundary values $\varphi_0(S) \equiv \varphi_0(a)$, $\varphi_0(b)$ are found from the two boundary conditions, which yield

$$\frac{\epsilon_\ell}{d}(\varphi_0(b) - \varphi_0(a)) - \epsilon_w\sqrt{2U[\varphi_0(b)]} = 4\pi\sigma_b$$

$$-\frac{\epsilon_\ell}{d}(\varphi_0(b) - \varphi_0(a)) - \epsilon_w\sqrt{2U[\varphi_0(a)]} = 4\pi\sigma_a, \tag{37}$$

where $\sigma_{a,b} < 0$ and the sign of the square-root terms have been chosen accordingly. The solution of this simultaneous system of equations gives $\varphi_0(a)$, $\varphi_0(b)$ to be used in the limits in the integrals of Eqs. 35 and 36.

If we had imposed boundary conditions such that the charge per midplane area was conserved during bending, the only change in Eq. 34 would be to replace the multiplicative

factor of b with R in the first term and, of course, to interpret $\sigma_{a,b}$ as the charge per midplane area. One can continue to employ the boundary conditions (Eq. 37), even though $\sigma_{a,b}$ are no longer the correct lipid-solution surface charges, by the argument already given that the surface value of φ_1 drops out. The only change to Eq. 20 is to remove the $d/2R$ factor multiplying $\sigma_{a,b}$.

TC thanks J. E. Evanseck for related discussions, and the authors thank W. Brown and M. Jarić for numerous helpful comments.

TC and EDS acknowledge the support of National Science Foundation grant DMR-9300711. MVJ acknowledges support from National Science Foundation grant DMR-9215231.

REFERENCES

Alberts, B., D. Bray, and J. Lewis. 1994. Molecular Biology of the Cell. Garland Publishing, New York.

Andelman, D. 1995. Electrostatic properties of membranes: the Poisson-Boltzmann theory. *In* Handbook of Biological Physics, Vol. 1, Structure and Dynamics of Membranes, Generic and Specific Interactions. R. Lipowsky and E. Sackmann, editors. Elsevier Science Publishers B.V., Amsterdam. 603–642.

Ben-Tal, N., B. Honig, R. M. Peitzsch, G. Denisov, and S. McLaughlin. 1996. Binding of small basic peptides to membranes containing acidic lipids: theoretical models and experimental results. *Biophys. J.* 71: 561–575.

Boggs, J. M. 1984. Intermolecular hydrogen bonding between membrane lipids. *In* Biomembranes, Vol. 12, Membrane Fluidity. M. Kates and L. A. Manson, editors. Plenum Press, New York.

Bretscher, M. S., and S. Munro. 1993. Cholesterol and the Golgi apparatus. *Science.* 261:1280–1281.

Chow, W. S., and J. Barber. 1980. Salt-dependent changes of 9-aminoacridine fluorescence as a measure of charge density of membrane surfaces. *J. Biochem. Biophys. Methods.* 3:173–185.

Cluett, E. B., S. A. Wood, M. Banta, and W. J. Brown. 1993. Tubulation of Golgi membranes in vivo and in vitro in the absence of Brefeldin A. *J. Cell Biol.* 120:15–24.

de Camilli, P., S. D. Emr, P. S. McPherson, and P. Novick. 1996. Phosphoinositides as regulators in membrane traffic. *Science.* 271: 1533–1539.

Dresner, L. 1963. A variational principle for the Poisson-Boltzmann equation. Activity coefficient of a salt in a charged microcapillary. *J. Chem. Phys.* 67:2333–2336.

Duplantier, B., R. E. Goldstein, V. Romero-Rochin, and A. I. Pesci. 1990. Geometrical and topological aspects of electric double layers near curved surfaces. *Phys. Rev. Lett.* 65:508–511.

Duwe, H. P., J. Käs, and E. Sackmann. 1990. Bending elastic moduli of lipid bilayers: modulation by solutes. *J. Phys. France.* 51:945–962.

Eibl, H., and A. Blume. 1979. The influence of charge on phosphatidic acid bilayer membranes. *Biochim. Biophys. Acta.* 553:476–488.

Gennis, R. B. 1989. Biomembranes: Molecular Structure and Function. Springer-Verlag, New York.

Gruenberg, J., and F. R. Maxfield. 1995. Membrane transport in the endocytic pathway. *Curr. Opin. Cell Biol.* 7:552–563.

Gruner, S. M., P. R. Cullis, M. J. Hope, and C. P. Tilcock. 1985. Lipid polymorphism: the molecular bases of nonbilayer phases. *Annu. Rev. Biophys. Biophys. Chem.* 211–238.

Honig, B., and A. Nicholls. 1995. Classical electrostatics in biology and chemistry. *Science* 268:144–149.

Hope, M. J., T. E. Redelmeier, K. F. Wong, W. Rodrigueza, and P. R. Cullis. 1989. Phospholipid asymmetry in large unilamellar vesicles induced by transmembrane pH gradients. *Biochemistry.* 28:4181–4187.

Hui, S. W. 1993. Lipid molecular shape and high curvature structures. *Biophys. J.* 65:1361–1362.

Israelachvili, J., S. Marcelja, and R. G. Horn. 1980. Physical principles of membrane organization. *Q. Rev. Biophys.* 13:121–200.

Lee, Y.-C., T. F. Taraschi, and N. Janes. 1993. Support for the shape concept of lipid structure based on headgroup volume approach. *Biophys. J.* 65:1429–1432.

Lipowsky, R. 1993. Domain-induced budding of fluid membranes. *Biophys. J.* 64:1133–1138.

Lippincott-Schwartz, J., J. G. Donaldson, A. Schweizer, A. Berger, E. G. Hauri, L. C. Yuan, and R. D. Klausner. 1990. Microtubule-dependent retrograde transport of proteins into the ER in the presence of brefeldin A suggests an ER recycling pathway. *Cell.* 60:821–836.

Marcus, R. 1955. Calculation of thermodynamic properties of polyelectrolytes. *J. Chem. Phys.* 23:1057–1068.

Miao, L., U. Seifert, M. Wortis, and H.-G. Döbereiner. 1994. Budding transitions of fluid-bilayer vesicles: the effect of area-difference elasticity. *Phys. Rev. E.* 49:5389–5407.

Mui, B. L.-S., H.-G. Döbereiner, T. D. Madden, and P. R. Cullis. 1995. Influence of transbilayer area asymmetry on the morphology of large unilamellar vesicles. *Biophys. J.* 69:930–941.

Mutz, M., and W. Helfrich. 1990. Bending rigidities of some biological model membranes as obtained from the Fourier analysis of contour sections. *J. Phys. France.* 51:991–1002.

Mitchell, D. J., and B. W. Ninham. 1989. Curvature elasticity of charged membranes. *Langmuir.* 5:1121–1123.

Petrov, A. G., and I. Bivas. 1984. Elastic and flexoelectric aspects of out of plane fluctuations in biological and model membranes. *Prog. Surf. Sci.* 16:389–512.

Rambourg, A., and Y. Clermont. 1990. Three-dimensional electron microscopy: structure of the Golgi apparatus. *Eur. J. Cell Biol.* 51: 189–200.

Rothman, J. E. 1994. Mechanisms of intracellular protein transport. *Nature.* 372:55–63.

Sack, F. D., D. A. Priestley, and A. C. Leopold. 1983. Surface charge on isolated maize-coleoptile amyloplasts. *Planta.* 157:511–517.

Schekman, R., and L. Orci. 1996. Coat proteins and vesicle budding. *Science.* 271:1526–1533.

Seifert, U., and R. Lipowsky. 1995. Morphology of Vesicles. *In* Handbook of Biological Physics, Vol. 1, Structure and Dynamics of Membranes, Generic and Specific Interactions. R. Lipowsky and E. Sackmann, editors. Elsevier Science Publishers B.V., Amsterdam. 403–464.

Sharp, K. A., and B. Honig. 1990. Calculating total electrostatic energies with the nonlinear Poisson-Boltzmann equation. *J. Phys. Chem.* 94: 7684–7692.

Shraiman, B. I. 1997. On the role of assembly kinetics in determining the structure of clathrin cages. *Biophys J.* 72:953–957.

Song, J., and R. E. Waugh. 1990. Bilayer membrane bending stiffness by tether formation from mixed PC-PS lipid vesicles. *J. Biomech. Eng.* 112:235–240.

Song, J., and R. E. Waugh. 1993. Bending rigidity of SOPC membranes containing cholesterol. *Biophys. J.* 64:1967–1970.

Tocanne, J.-F., and J. Teissié. 1990. Ionization of phospholipids and phospholipid-supported interfacial lateral diffusion of protons in membrane model systems. *Biochim. Biophys. Acta.* 1031:111–142.

Terasaki, M., L. B. Chen, and K. Fujiwara. 1986. Microtubules and the endoplasmic reticulum are highly interdependent structures. *J. Cell Biol.* 103:1557–1568.

Trowbridge, I. S., J. F. Collwan, and C. R. Hopkins. 1993. Signal-dependent membrane protein trafficking in the endocytic pathway. *Annu. Rev. Cell Biol.* 9:129–161.

Winterhalter, M., and W. Helfrich. 1988. Effect of surface charge on the curvature elasticity of membranes. *J. Phys. Chem.* 92:6865–6867.

Winterhalter, M., and W. Helfrich. 1992. Bending elasticity of electrically charged bilayers: coupled monolayers, neutral surfaces, and balancing stresses. *J. Phys. Chem.* 96:327–330.